International Journal of Physical Research, 10 (1) (2022) 1-17

International Journal of Physical Research

Website: www.sciencepubco.com/index.php/IJPR
DOI:10.14419/ijpr.v10i1.31874

Research paper

A ½ spin fiber model for the electron

Emmanouil Markoulakis [1] *, Emmanuel Antonidakis [1]

[1] Department of Electronic Engineering, Computer Technology Informatics & Electronic Devices Laboratory, Hellenic Mediterranean University, Romanou 3, Chania 73133, Crete, Greece
**Corresponding author E-mail:markoul@hmu.gr*

Abstract

The Standard Model and Quantum Mechanics studies the quantum world as a collection of probabilistically interacting particles and does not tell us what a single isolated particle like the electron is, thus its intrinsic detailed field mechanics and how these are generating its intrinsic property values like charge, spin, magnetic moment and handedness. We herein are translating these intrinsic physical properties of the electron to a novel 4-dimensional (i.e. three spatial plus one temporal) fiber spinor and showing their possible deeper correlation and interconnection combined under a single energy manifold. From physical quantum emulation observations, mathematical analysis and Wolfram Alpha parametric polar simulations and mathematical 4D animations we calculated a fiber model for the dressed bare mass electromagnetic field of the electron that results to all of its known measured intrinsic properties. Therefore our model is an intrinsic mechanics model for the electron at rest and shows the possibility that the elementary electron although it has no inner sub-particles, it can posses a specific energy flux manifold. Why an electron is actually a ½ spin geometry, twisted photon. The fine structure constant is explained as a topological feature, proportionality constant, embedded inside our proposed fiber model for the electron. Our novel fiber model opens up a new door on theoretical intrinsic mechanics physics of elementary particles beyond the Standard Model.

Keywords: *Elementary Particle Physic; Electron Manifold and Topology; Intrinsic Properties of Electron; Beyond Standard Model Physics; Fiber Model of Electron.*

1. Introduction

Our theoretical research presented herein, is based on our previous published experimental observations which we reference and describe briefly also in here and can be described as part of a Topological Quantum Field Theory (TQFT) and in particular to the research fields of four-dimensional spinors and strings. This research proposes a manifold for the electron combining four-dimensional spinors with strings referring to the novelty of our research and therefore a complete description of the electron as a quantum string spinor.
Also, we have like to state here that our paper does not in any way contradict or tries to replace the standard Model (SM) but the aim of our research is to complement the SM by describing a novel possible physical procedure and mechanism which is responsible for producing the measured known values of the intrinsic properties of the electron like spin, charge and magnetic moment. Therefore, describing the origin of these intrinsic properties and their deeper correlations with each other. The SM describing these properties like spin, as "intrinsic" is admitting that we do not actually know by which mechanism these properties have come to be. In our paper we try to decipher the origin of these properties by presenting a topological manifold of the electron extrapolated by actual experimental data which its observed topological and geometrical features correspond and correlate to the intrinsic properties of the electron.
The final proposed manifold for the electron by our analysis presented, is fine tuned by back engineering the known measured values of the electron predicted by the SM like its total spin angular momentum and geometrically fine tuning with these the proposed manifold for the electron. The Wolfram simulated results are very consisted with the predicted SM values for the electron like the Compton wavelength frequency ≈1.24E20 Hz and the reduced Compton wavelength ƛ ≈3.86E-13 m and also our model makes additional more accurate prediction of the actual charge radius for the electron at rest explaining why the reduced Compton wavelength ƛ known value using light scattering methods is larger than the actual simulated in the proposed manifold, charge radius of the electron value of 3.344E-13 m. (see section 3.2).
In general we should regard quantum mechanics and present quantum field theory as formal physical theories predicting accurately physical outcomes, thus, results of the microscopic world (and also in most cases the macroscopic in extension) but not made to describe all the actual physical processes leading to these results (i.e. we can reach the same numerical values, results, by different algorithms and mechanisms). With other words, all these in the sense regarding physical processes, are merely effective theories and basically the actual mechanics describing these physical processes are unknown to us.
Here comes the beyond the standard model branch of physics like for example string theory or quantum gravity or topological quantum field theories, to try to give these answers. Our research is in the above described direction and which is also additionally based in previous related published experimental data also outlined herein, has merits and can give a precious deeper insight of the electron beyond the SM and potentially useful conclusions for deciphering some of the yet "mysteries" of the quantum that SM seems to struggle with.

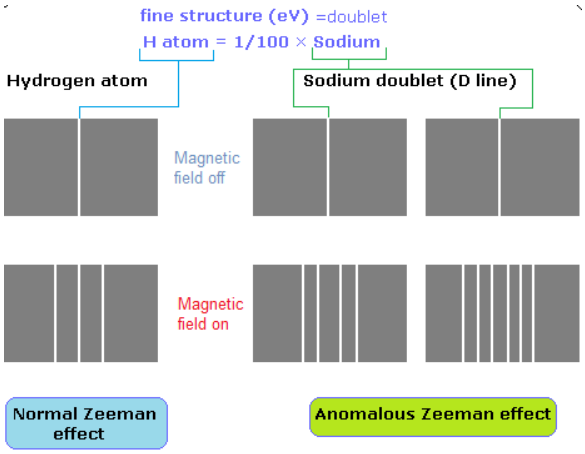

Fig. 1: The Anomalous Zeeman Effect.

We try in our research to complement the SM (i.e. using a novel 4-dimensional quantum string spinor) by deciphering the origin of the intrinsic properties of the electron and unifying them under a single energy manifold.

When Goudsmit and Uhlenbeck formally introduced first the theory [1] [2] of a spin angular momentum the electron must possess besides its known orbital angular momentum by doing so they introduced at that time a "forbidden component", m_s spin quantum number (i.e. in a subsequent paper by L.H. Thomas [3] it was proven how this apparent violation can be lifted). It is a well known practice because macroscopic calculations when applied to the quantum, result often to irrational and inconsistent results and infinities, therefore quantum mechanics applies restrictions and things you are not allowed do and are forbidden. Despite that, they boldly went on and published their findings because they perfectly accounted for some unexplained observations by spectroscopers regarding the Zeeman Effect [4].

Spectroscopists observed "anomalous" splitting [5] [6] in the previously studied "normal" Zeeman Effect, sometimes with unequal spacing, fig. 1.

Additionally, some energy levels show splitting that resembles the Zeeman Effect even when there is no external magnetic field. For instance, when hydrogen spectral lines are examined, some spectral lines are found to consist of sets of closely spaced lines called multiplets. Experiments such as the Stern-Gerlach experiment [7] [8] showed that particles are found to posse's angular momentum that cannot be accounted for the orbital angular momentum alone. This led the two Dutch scientists, Goudsmit and Uhlenbeck, to propose that electrons may have additional motion. Using a semi-classical model, they suggested the electrons behave as a sphere of charge that spins about its own axis. If so, it would have an additional spin-angular momentum and magnetic moment related with, which if quantized as well, would explain the observed energy level anomalies.

In the presence of an external magnetic field, this spin magnetic moment would interact in addition to that due to the orbital magnetic moment. Therefore, this spin magnetic moment is responsible for the "anomalous" Zeeman shifts. Precise further experiments, have conclusively shown that electrons do indeed have a spin angular momentum and an associated spin magnetic moment that do not depend on orbital motion.

However, there is a contradiction. No actual size has been ever found or measured for electrons. They appear to be dimensionless point particles and therefore they should not be able to physically spin about their axes. All reported radius in literature for the electron so far, the classical electron radius [9], the Compton radius for the electron [10] [11] and the Bohr radius of the electron [12] are all effective radii and not the actual physical and are extrapolated and derived from other parameters and equations. The theoretical difficulty for finding a hypothetical actual radius assuming a spherical electron at rest and defined as the volume in a three-dimensional Euclidean space, its conserved steady rest mass occupies, is that it is ultimately determined by the electron's mass total intrinsic spin angular momentum known value of 0.866ħ. However, this value depends on the product of the angular velocity times the radius which can be any arbitrary combination within the light speed limit c.

Nevertheless, electrons do have an additional angular momentum that is not associated with orbital motion. The way out of this conflict? Based on the above arguments, the consensus is that electrons being point particles do not physically spin. The origin of the "spin" angular momentum is therefore, fundamentally quantum mechanical in nature and it is intrinsic to the electron. With other words, the physical process by which the electron generates its spin angular momentum is hidden and unknown.

The authors of this paper find the above conclusion non-satisfactory and more like a compromise, outlining our inability to measure experimentally any size for the electron and explain the intrinsic mechanism and origin if its spin angular momentum. We will show later on using effective geometry and topology based and extrapolated from actual experimental observations and taking into consideration that the near field of the electron charge was actually measured with great accuracy [13] and found to be spherical symmetrical and homogeneous without any electric dipole moment present, that there is no other way the electron to get its total intrinsic spin angular momentum of $(\sqrt{3}/2)\hbar \approx 0.866\hbar$ known value, without physical rotation involved around the center of mass. Therefore, the conserved effective rest mass of the electron occupies a volume in space and thus the electron has size at rest.

Moreover, we found by examining the resulting energy flow spin relativistic manifold of the electron which is based on our experimental observations, besides its ½ spin intrinsic angular momentum component (i.e. projection) of the electron, a so called second "forbidden" $(1/\sqrt{2})\hbar$ intrinsic spin angular momentum component effectively perpendicular to the first component and rotation, involving a second hidden intrinsic to the electron rotation, along its magnetic moment N-S axis of its dynamic manifold we call revolution to distinguish it from the first component rotation. Our analysis herein leads to the inescapable conclusion that the total intrinsic spin angular momentum of the electron 0.866ħ is the vectorial sum of these two spin angular moment components (i.e. including the newly found) of the electron and their involved rotations. Evidently, we show that when these two, the $L_S=m_S\hbar=(1/2)\hbar$ and the newly found in the manifold $L_R=m_R\hbar=(1/\sqrt{2})\hbar$, spin angular momenta components, are combined to calculate the total mass spin angular momentum vector of the electron manifold $L(e)= (\sqrt{3}/2)\hbar \approx 0.866\hbar$ then the well known value reported in particle physics literature [14–17], $L(e)\angle 54.7°$ vector angle of the total mass of the electron's spin angular momentum L(e) to the electron's magnetic moment N-S axis, pops out from the calculations of the proposed manifold.

We discuss following, why we believe albeit the restriction applied by quantum mechanics that we are not allowed to examine more than one spin angular momentum component at the time hence we are not allowed to combine different spin angular moment components due the Heisenberg Uncertainty principle [18], our proposed effective manifold cannot be subject of this principle that prohibits the notion of a quantum particle literally "spinning" about an axis since our effective topology and manifold analysis is not a standard model quantum mechanics analysis and research and we are not bound by its restrictions. Our proposed manifold describes the mechanics inside the electron beyond the Standard Model (SM) physics where the SM has no grasp and our research can categorized as such, beyond the Standard Model research.

We examine the free electron at rest in the proposed manifold, fundamentally as a closed isolated system where there is no external quantum noise present from the environment and no quantum decoherence [19–21]. All elementary physical properties of the electron like mass, charge, spin, magnetic dipole moment and their origin and correlations are shown in the manifold as topological and geometrical dynamical features embedded in this manifold and their known values extrapolated from it. Also the fine structure constant is shown how it may be possible to be embedded as a proportionality constant of the topology and geometry of the proposed manifold of the electron.

With that said, our research however can act as a bridge between quantum mechanics and string theory since it has shown that the photon which has a spin 1, can be considered topologically as a two dimensional ring or closed loop revolving string (i.e. we prefer to refer it also as energy ribbon) without volume which therefore does not interact with the Higgs field [22][23] and thus has no mass hence it can propagate with speed c through spacetime whereas an electron topologically is actually a ½ spin twisted photon (i.e. a multiple twisted in three dimensions closed loop string) that spins and revolves around its center axis at relativistic speeds locally and therefore in contrast to the spin 1 photon, occupies a volume in spacetime, therefore it can interact with the Higgs field and gain its mass inertia which prohibits the electron to travel through spacetime with a linear speed c.

This realization from our research strongly infers that elementary particles cannot have mass and interact with the Higgs field, without occupying a volume in 3D Euclidean space and therefore the electron cannot be dimensionless. Giving volume, topology and an energy flow manifold description to the electron we deem necessary in order to understand and decipher the origin of its intrinsic properties like electron spin, charge and its magnetic dipole moment and explain physically their correlations.

2. Electron manifold

2.1. Physical interpretation

Based on our previous research [21] [24 - 26] and continuously refining it over the span of the last four years, using a quantum magnetic optic non-magnetohydrodynamic ferrolens, physical magnetic flux viewer device which has a very small decoherence [21] factor and looking inside the bulk matter of ferromagnets, we were able to obtain in real time the two-dimensional stationary electromagnetic flux imprint of the unpaired and aligned electron inside the ferromagnet's bulk matter. In other words, the Quantum Magnet electromagnetic flux 2D projected manifold of a hypothetically stationary electron at rest (i.e. stationary magneton) [21]. The novel idea behind this was, since we are not capable with today's instrumentation and because most importantly the Heisenberg Uncertainty principle to actually see the electromagnetic flux of a single electron as we would see it in a normal macroscopic magnet in the classical iron filings experiment, maybe instead we could use a normal magnet as our "giant magnification microscope". The dipole magnet would emulate successfully a static electromagnetic flux manifold of the single electron of all the aligned unpaired electrons inside the magnet whenever viewed with a quantum magnetic optic device which would have minimum decoherence like the ferrolens. The last part is very important and key to the whole experiment. We have found that the final classical dipole magnetic field on air of a ferromagnet we are familiar, is due a quantum decoherence process.

In fig. 2(a) a magnet is horizontally placed N-S poles, left to right (i.e. vortex black holes are where its two poles of the magnet are located) under the ferrolens. The ferrolens's 10nm in average size magnetic sensors exhibit minimum decoherence and therefore allow us to see the Quantum Magnet field inside our macroscopic magnet (see colored thick spiral lines).

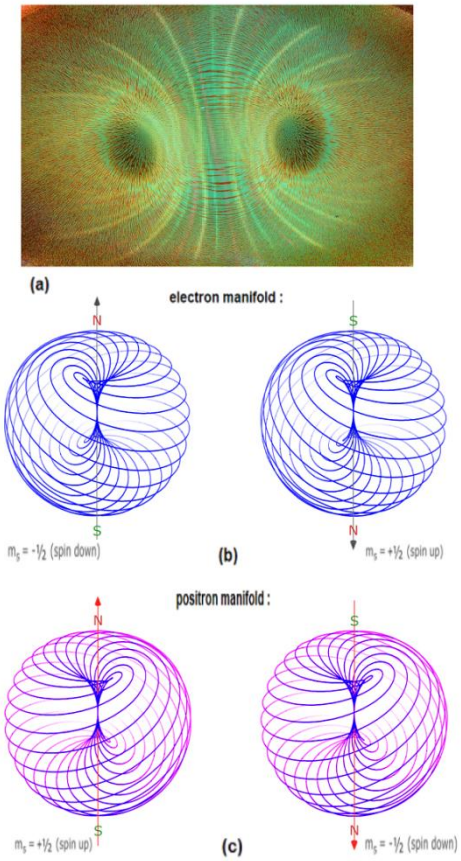

Fig. 2: (a) The Quantum Magnet non-decohered electromagnetic flux 2D imprint shown in real time of a macroscopic dipole magnet placed under the ferrolens *(see thick multicoloured lines, black holes are the locations of its two poles)* against its decohered classical N-S magnetic flux imprint shown with iron filings (see thin brown lines) [21, fig.3]. (b) Static Illustration of the spin relativistic electromagnetic flux 3D manifold of the electron as interpreted form its 2D imprint on the ferrolens shown previously in fig. 2(a), when projected in 3D Euclidean space. Both spin down m_s= - ½ and spin up m_s= + ½ versions of the electron manifold are illustrated. Because the negative charge –e electron, the ½ spin vector z-axis projection is antiparallel to the magnetic moment vector (S to N inside the electron). (c) Same as (b) but this time the positron the antimatter counterpart of the electron. Because the positive charge +e positron, the ½ spin vector z-axis projection is this time in contrast to the electron case, parallel to the magnetic moment vector. (b)&(c) See in this link here https://tinyurl.com/y3pyoal4 [28] an animation of the dynamic model of the proposed manifold.

At the same time we sprinkle above the lens some iron filings thus performing the classical experiment (see thin brown lines). The decoherence process taking place is here clearly shown. The relative macroscopic hundreds micron sized iron filings magnetic sensors are subject to strong decoherence and therefore imprint the classical familiar N-S axial field of the magnet, in contrast the nanosized much less susceptible to decoherence magnetic sensors inside the ferrolens successfully imprint the Quantum Magnet field hidden from normal macroscopic sight. Using the above described method of a macroscopic magnet as an emulator in conjunction with the quantum optic ferrolens we circumvent both obstacles of the Heisenberg Uncertainty principle [18] and the decoherence [19-21] problem and we are now able to obtain a static 2D imprint of the electromagnetic flux manifold of the single electron at rest (see fig.2a thick colored lines). Moreover, as a very important bonus in our research, no similar to other quantum sensors and methods like the SQUID micron-resolution Magnetic Scanning Microscope [27] where the magnetic imprint of a subject sample is obtained as a cloud pattern therefore only geometric features of the imprint can be observed, with the ferrolens we can observe discrete magnetic flux lines allowing us therefore in our case to observe in addition the topology and manifold of the electron's stationary imprint magnetic field (i.e. magneton).

In fig.2(b) we see a basic static illustration of the proposed spin relativistic electron 3D manifold and its counterpart antimatter positron in fig. 2(c) as extrapolated from the 2D imprint of fig. 2(a) on the ferrolens. The actual dynamics of the proposed manifold are illustrated in this animation here, https://tinyurl.com/y3pyoal4 [1] [28]: A relativistically latitude revolving effectively in the z-axis, and through the N-S magnetic moment axis with F_R angular velocity and longitudinally spinning with F_S angular velocity along the xy-axes and around the magnetic N-S moment axis, electromagneto sphere of spiralling electromagnetic flux (see animation of F_R and Fs components, https://tinyurl.com/y8t4d6w8 [2]). Overall, a ½ spin manifold. The intrinsic spin helicity and handedness differences between the electron and positron manifolds are also demonstrated in the above animation link.

In our research and proposed manifold, there is no really any physical ontological distinction between the electron's charge and the electron's magnetic flux. Their difference is only in the spatial orientation in motion. The horizontal projection rotational motion component on the xy-plane of the magnetic flux lines thus the longitudinal rotation at F_S angular frequency of the magnetosphere, represents the electron charge whereas the vertical rotational motion component on the z-axis of the magnetic flux lines, thus the continuous revolution of the magnetic flux lines through the diametrically double horn formation of the manifold at angular frequency F_R, shown in the above animation link, represents the N-S magnetic moment of the electron.

These two relativistic speed rotation projections of the electromagnetic flux lines in the manifold are perpendicular to each other and create the perpendicular radiated electric E-field vector and magnetic M-field vector of the electron thus the origin for the Electromagnetism phenomenon. Both of these energy rotations of electromagnetic flux combined, as we will show later on in our analysis, create the mass inertia of the electron via the interaction with the Higgs field and centered at a point at the center of the proposed manifold's double

[1] https://web.archive.org/web/20201231123500/https://www.horntorus.com/particle-model/mm-index.html (permalink)
[2] https://web.archive.org/web/20210527160257/https://www.horntorus.com/particle-model/standarddynamichorntorus_10.html

horn formation. The center of the manifold is the center of mass (see fig. 2) and also there where all the mass of the electron is located and focused. Therefore by all means, the actual rest mass and center of rest mass of the electron are one and the same thing and can be regarded as a dimensionless point occupying no volume in space, however the electron's energy manifold corresponding to its rest mass occupies a localised volume in space and therefore the electron itself is not dimensionless and has a charge radius (i.e. radius of the manifold). If the electron had no volume in space it would never be able to interact with the Higgs field in the first place and therefore it would had no mass.

There is also an unanswered question about the origin of the magnetic lines of force? If the magnetic flux lines on a ferromagnet are created due the exchange interaction of virtual photons as it is believed, among the aligned unpaired electrons inside the bulk material of the ferromagnet, then what creates the magnetic flux lines or else called, the magnetic lines of force on a single electron at rest? The authors herein, especially after succeeding experimentally to create an emergent synthetic monopole [24] just by the mere act of topologically manipulating magnetic flux lines, believe that electromagnetic lines of force (i.e. streams of virtual photons) are not an emergent phenomenon of the electron but mediated by it and the real origin of these is the fabric of spacetime itself or else vacuum space and manifested whenever this is disturbed. In that sense the electron is a spontaneous spatial and temporal distortion of vacuum space or else regarded in quantum theory, as an excitation in the quantum fields. The electron does not originally create the electromagnetic flux. Instead, these whirling and spinning electromagnetic lines of force create the electron.

Therefore, this spin relativistic electromagnetic flux manifold presented herein, is the electron. Another physical realization by observing our experimentally based proposed electron manifold shown in fig.2, is that the nature of the magnetic moment of the electron is not Amperian (i.e. single loop of charge creating a magnetic dipole moment) but rather Gilbertian [29] thus as shown in the manifold, created by two discrete relative counterrotating monopole vortex magnetic flux charges in a joint dipole spherical vortex formation. Their joint is the vortex string or as we prefer to call vortex tube, thus the double horn formation inside our manifold shown which represents the magnetic dipole moment of the electron. This is also backed up by our previous experimental research [24] where when we forced magnetic flux lines into a single vortex topology, an emergent synthetic Dirac magnetic monopole was emulated out of the blue which we have measured. The quantitative relation of the magnetic dipole charge $q_{\mu e}$ in SI (A·m) units, flowing through the magnetic moment axis , thus horn tube in the proposed manifold, relative to the electron charge e, on the surface of the manifold is shown in the equation (1) we have derived, (analytic solution of this equation can be found at the Appendix [28]) :

$$q_{\mu_e} = ec \tag{1}$$

Where c is the speed of light in vacuum space. Topologically equation (1) on the manifold, translates as the surface m^2 area of the manifold that flows per unit of time m^2/s through the double horn formation thus magnetic moment of the electron (see animation https://tinyurl.com/y3pyoal4).

Coming now back to the two combined F_S and F_R projected rotations of the manifold these are easily visualized in fig. 3 showing the Lissajous trajectory path of any point on the manifold's magnetosphere using a closed loop quantum string or as we prefer to call it, an energy ribbon representation. The dynamic manifold of the energy ribbon is shown in this animation link here, https://tinyurl.com/ya2qvx9a [3]. All the intrinsic properties of the electron are generated by this revolution F_R motion and rotational F_S motion of this single energy ribbon of fig.3(a) (see animation of F_R and F_S components, https://tinyurl.com/ttbvkx6 [4]). The ribbon returns to its initial state after 720° of F_S rotation as fermionic behaviour dictates. This energy ribbon is actually a twisted in 3D Euclidean space loop of electromagnetic flux that revolves and spins at the same time, with tangential velocity c, for any point on the ribbon and to any spatial direction. It is therefore a ½ spin manifold photon. This relativistic speed c combined motion of this single energy ribbon shown in fig.3(a) creates the spin relativistic magnetosphere manifold and charge of the electron shown in fig.3(b)&(c) (animation of F_R and F_S components, https://tinyurl.com/y8t4d6w8). The whole electron magnetosphere manifold, because it has gained volume, thus, it cannot move with linear speed c through space is interacting now with the Higgs field and gains therefore its mass inertia. In contrast a 2D without volume spin 1 photon which its manifold shown in fig.3(d), can move linearly through space effortlessly at speed c. As a matter of fact c is the only speed the photon can move, even inside condensed matter else it ceases to exist.

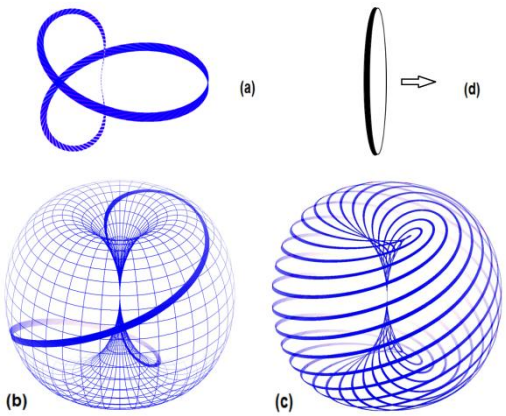

Fig. 3: (a) The Lissajous trajectory path of the electron manifold, energy ribbon (i.e. quantum string spinor) or else ½ spin photon. Its dynamic manifold is demonstrated in this animation link here, https://tinyurl.com/ya2qvx9a, ribbon returns to its initial state after 720° of rotation as fermionic behaviour dictates (b) the previous trajectory path depicted in fig.3a is shown inside the spherical volume of the electron manifold. (c) This single energy ribbon or else called quantum string shown in fig.3a above which is actually a ½ spin photon manifold, when revolved vertically and span horizontally relativistically at speed c then creates the spin relativistic magnetosphere manifold of the electron shown here in fig. 3c. (d) For comparison, the manifold of a normal spin 1 photon (i.e. a 2D closed loop of electromagnetic flux) revolving like a "bike wheel" along its perimeter at tangential speed c and also travelling through Euclidean 3D space at linear speed c from left to right as shown.

[3] https://web.archive.org/web/20201231124624/https://www.horntorus.com/particle-model/e_spin-up.html (animation permalink)
[4] https://web.archive.org/web/20210526094105/https://www.horntorus.com/particle-model/revolution-rotation-superposition.html

Additionally, here in this animation, https://tinyurl.com/y8hqa6sp [5] a virtual photon exchange is demonstrated between two relative nearby electrons. A virtual photon is ejected from one electron and the virtual photon is shown how it unfolds during its exit from the electron from a ½ spin manifold inside the electron to a spin 1 manifold and travels across to the other electron which then absorbs this virtual photon and integrates it to its charge. It is very important to understand for this research presentation at this point, that any point on the electron revolving and spinning magnetosphere manifold and energy ribbon, moves with a steady and fixed tangential velocity c. Therefore our proposed manifold is called spin relativistic.

Lastly, for section 2.1 of the physical interpretation of the proposed electron manifold, we left the previously referenced in the Introduction section, the known to elementary particle physics L(e)∠54.7° angle existing, of the intrinsic total mass spin angular momentum pseudo-vector L(e) ≈0.866ħ of the electron to its N-S magnetic moment axis. This angle α°=54.73561° more accurate value, referenced also formally in mathematics and physics with the name, the magic angle [30], has proven in our research of pivotal importance, and key for binding the proposed manifold with the known physical properties of the electron as we will show in the next sections. This α° specific angle is reflected in the manifold's electromagnetic flux lines, as a tilt angle they all have towards the L(e) total spin mass angular momentum of the electron relative to its magnetic moment N-S axis as shown in fig. 4(a). Not all electromagnetic flux lines have this same exact α° angle all over the manifold since their angular velocity varies and increases towards the poles of the manifold but their tilt angle becomes exactly α°=54.73561° at the exact time they cross the equatorial plane of the manifold where the center of mass of the electron is located, at the center of the proposed manifold.

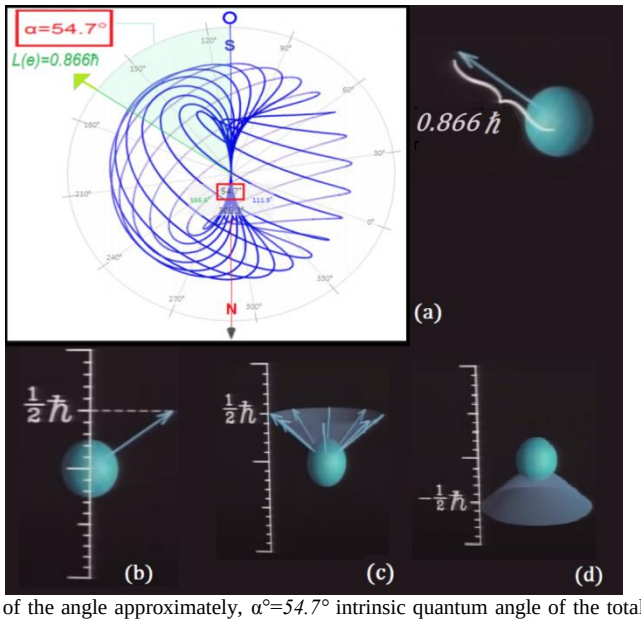

Fig. 4: (a) Illustration with a protractor of the angle approximately, α°=*54.7°* intrinsic quantum angle of the total spin of the mass of the electron *L(e) ≈0.866ħ* pseudo-vector to its magnetic moment N-S axis positioned on the z-axis vertical frame of reference, which is reflected in the proposed manifold as a tilt angle of the electromagnetic flux lines at the exact value of α°=*54.7°*, whenever passing the equatorial plane of the manifold where the center of mass is located at the center of the magnetosphere. This particular illustration shows the case of a +½ spin up electron. Notice, that because the negative charged –e electron, its magnetic moment vector S to N (inside the electron) is pointing in an antiparallel region in space relative to the *L(e)* vector. (b) The z-axis spin projection component ħ/2 of a spin up m_s =+ ½ quantum number electron. (c)&(d) The *L(e)* total spin vector direction of the electron can vary anytime due the Heisenberg Uncertainty principle but can only be positioned on the surface of the cone shown, which has always an α°=*54.7°* angle to the vertical. Depending of if this cone is facing up or down, we characterize the electron as spin up or spin down.

It is hard here not to notice from fig.4 (a) the similar pattern with the Earth's Magnetic South Pole located on the geophysical North Pole region of the Earth with an inclination angle to the physical spin axis of the Earth and the Magnetic North Pole of the Earth located on its geophysical South Pole. Similar behavior is also observed in the electron manifold of fig.4(a) because the negative –e electron charge, it points its magnetic moment vector in an opposite region relative to its total mass spin vector L(e) (i.e. S to N direction inside the electron manifold of moving electromagnetic flux through the horn tube and N to S direction of the electromagnetic flux lines moving outside the manifold on its surface) . However, a positive charged particle +e like the positron will exhibit in contrast to the electron's antiparallel behavior, a parallel behavior having its magnetic moment vector pointing to the same region where the total spin vector L(e)=0.866ħ of the positron is located. Generally, we say that the electron's magnetic moment N-S, is antiparallel to its spin angular momentum z-axis projection component vector L_S= (½) ħ. This situation is best demonstrated in this animation link https://tinyurl.com/y3pyoal4 of fig.2 presented manifold, simulating its dynamic behavior and also in this animation, https://tinyurl.com/ycxjr39z [6] but notice now in this model animation the spatial vertical frame of reference is not the magnetic moment N-S axis of the electron but is shifted towards its total spin L(e) ≈0.866ħ axis which now is shown in the vertical spatial direction instead.

Fig. 4(b) shows the z-axis component projection of the electron's total spin L (e) =0.866ħ, thus L_S= (½) ħ spin angular momentum which is associated with a F_S angular velocity and r_S spin charge radius. In the following sections we will show formally and physically in the proposed manifold that the above vector value 0.866ħ and its associated angle L(e)∠α°=54.7° is not possible without the introduction of a second spin angular momentum component which is manifesting naturally from our manifold and calculations , of L_R=(1/√2)ħ projected on the x-axis for any given instance on the xy-plane which is associated with the revolution of the electromagnetic flux through the horn tube of the manifold thus magnetic dipole moment of the electron. This L_R spin angular momentum component projection has an effective F_R angular velocity assigned to it and an effective magnetic moment revolution radius r_R. In Fig.4(c)&(d), it is shown that the L(e) total spin vector direction of the electron can vary anytime its position on the xy-plane due the Heisenberg Uncertainty principle but

[5] https://web.archive.org/web/20201231125418/https://www.horntorus.com/particle-model/EMs-virtualphoton.html (slow animation)
[6] Permalink https://web.archive.org/web/20201231131412/https://www.horntorus.com/particle-model/phi-hornspheroid_7-8.html (slow animation loading time)

can only be positioned on the surface of the cone shown, which has always an α°=54.7° angle to the vertical. Depending of if this cone is facing up or down, we characterize the electron as spin up m_S=+½ or spin down m_S=–½.

2.2. Spin angular momenta analysis

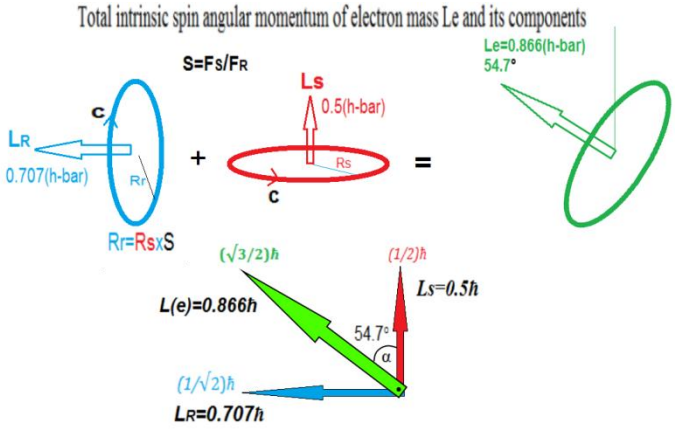

Fig. 5: Graphical analysis of the *effective* spin angular components of the total *L(e)* spin angular momentum of the electron manifold and their associated corresponding angular velocities F_S and F_R and radii R_S, Rr. Tangential velocity in all cases is c, the speed of light.

We are here now will present an analysis of the total spin angular momentum L (e) of the electron dynamic manifold and its projected components L_S and L_R discussed in the previous sections by calculating their effective point mass orbital translation associated radii and angular velocities using the parallel axis theorem and applying a fixed tangential velocity in all cases of c, the speed of light. We examine in our analysis the manifold for a spin up m_S=+½ electron. To aid our analysis we present also the graphical illustration of fig.5.
From the above information of fig.5 we get:

$$\tan a = \frac{L_R}{L_S} = \sqrt{2} \tag{2}$$

With,

$$a^\circ = \arctan\sqrt{2} = 54.73561^\circ \tag{3}$$

Therefore eq. (2) and (3) are the spin angular momentum consistency criterion check we will use later on in the paper to find out the exact parametric equations for the manifold describing the electron at rest. Notice here that $L_R/L_S=\sqrt{2}$ will always result in α°=54.73561° and vice versa.
Also, because the fixed light speed c, using the equation $c=2\pi f\cdot R$, where f is the angular velocity frequency and R the radius of the rotation and $P=2\pi R$ the perimeter of the rotation with c being the fixed value of the tangential velocity of the rotation the following equation must hold,

$$\frac{F_S}{F_R} = \frac{P_R}{P_S} = \frac{R_r}{R_S} \tag{4}$$

In order our manifold to be consistent with the speed of light c. Therefore eq. (4) is our light speed consistency criterion check for choosing the exact parametric equations for the manifold describing the electron.
Both criteria above described, thus equations (2), (3) & (4) must be obeyed in order our proposed manifold to correctly describe the electron at rest. For ease we name the frequency ratio F_S/F_R from now on,

$$S = \frac{F_S}{F_R} \tag{5}$$

With,

$$R_r = S \cdot R_s \tag{6}$$

The energy of monochromatic light is described by the Planck equation E=N·hf where N an integer number of photons and the single photon of spin 1 having a spin angular momentum of (1· ħ) and the energy of a single photon being $E_{Ph}=hf_{Ph}$ for N=1. The f_{Ph} in the equation is the angular velocity frequency of the single photon in the monochromatic light (i.e. all photons having the same wavelength λ) as we have described the single photon previously in fig.3(d) as a revolving like a "bike wheel" spin 1 circular closed 2D loop with its wavelength $\lambda_{Ph}=P_{Ph}=2\pi R_{Ph}$ being the perimeter P_{Ph} of its circular loop topology (see fig.3d). Therefore, $f_{Ph}=c/\lambda_{Ph}=c/(2\pi R_{Ph})$ where R_{Ph} is the radius of its closed loop topology shown in fig.3(d).
Although there are many different wavelength photons, all electrons at rest are exactly the same with each other giving out the same effective λ_C Compton wavelength and Compton radius for the electron $R_C \approx 3.86E\text{-}13m$ when transformed effectively from a ½ spin topology to a spin 1 topology (see animation link https://tinyurl.com/y8hqa6sp).
Therefore, we can use the Plank equation which is standard model Quantum Mechanics equation, for monochromatic light photons given above, E=N·hf, but transformed to calculate the energy of electrons instead but only for one spin angular momentum projection component at a time due to the Heisenberg Uncertainty principle restriction imposed, meaning that it cannot be used for calculating the corre-

sponding energy of the total spin L(e)=(√3/2)ħ ≈0.866ħ vector since it is product of vectorial sum of L_S and L_R spin components. Also notice here, that the total spin angular momentum for any electron at rest is always ≈0.866ħ, thus less of the spin angular momentum of a single photon which is ħ. That is expected since an electron as we described previously in section 2.1, is a twisted ½ spin photon topology thus a twisted loop manifold whereas a photon is a circular loop topology and therefore a photon can achieve always more spin angular momentum than the electron at rest for the same angular velocity frequency and radius values (i.e. a circular loop compared with a twisted loop of the same perimeter, produces always more angular momentum for the same value of tangential speed of rotation).
From our above analysis, the Planck light equation can now be transformed to describe the corresponding energy E_S of the z-axis L_S spin component of a single electron at rest by the following equation:

$$E_S = \frac{1}{2} \cdot hF_S \tag{7}$$

Where the ½ number is the Ls spin. We will use eq. (7) later on to calculate the energy of the F_S rotation.
The effective radius corresponding to the total spin angular momentum of the electron L(e) is calculated by the following equation,

$$L(e) = 0.866\hbar = m_e \cdot c \cdot r_e \tag{8}$$

Where m_e is the reported rest mass of the electron and c the speed of light. Solving for r_e, gives us an effective circular loop radius corresponding to the total spin angular momentum of the electron of an approximate rounded up to three decimal digits value equal to,

$$r_{e(\text{eff})} = R_S = 3.344 \cdot 10^{-13}(\text{m}) \tag{9}$$

In our proposed model the effective radius of the electron is the charge radius (i.e. radius from the center of the manifold) therefore r_e(eff)=R_S and considering a fixed tangential velocity the speed of light c, then F_S spin angular velocity to be approximate rounded up value of,

$$F_S = \frac{c}{2\pi r_e} = 142.67 \cdot 10^{18}(Hz) \tag{10}$$

Using eq. (7) and (10) we find the corresponding energy of the F_S rotation,

$$E_s = 4.727 \cdot 10^{-14}(J)(0.295\text{MeV}) \tag{11}$$

Knowing the total energy of the electron at rest of 0.511MeV and converting it to Joules we now can calculate using the conservation of energy, the energy of the F_R x-axis component rotation,

$$E_R = E_e - E_S = 3.46 \cdot 10^{-14}(J)(0.216\text{MeV}) \tag{12}$$

We are now able to calculate the effective circular loop radius R_r(eff) of the x-axis spin angular component L_R,

$$L_R = \frac{1}{\sqrt{2}}\hbar = \frac{E_R}{c} \cdot R_{r(eff)} \tag{13}$$

Thus,

$$R_{r(\text{eff})} = 6.46 \cdot 10^{-13}(\text{m}) \tag{14}$$

Solving equation (7) for spin 1/√2 and substituting the value E_R found in eq. (12) we finally can calculate also the effective angular velocity frequency for the F_R rotation,

$$F_{R(\text{eff})} = \frac{E_R}{\frac{1}{\sqrt{2}}h} = 73.85 \cdot 10^{18}(\text{Hz}) \tag{15}$$

All found parameter values of R_S, F_S, R_r and F_R found in eq. (9),(10), (14) and (15), comply with the light speed c consistency check of equation (4).

2.3. Parametric analysis

The only dipole topology and geometry which effectively could physically emulate a spinning ball of charge with a magnetic moment running diametrically through the poles, is the general topology of the horn torus [31] (https://tinyurl.com/ydz35wwh) and spirals on spherical surfaces [32] with the charge flowing through its double horn formation (i.e. dipole vortex string or vortex tube) effectively emulating the magnetic moment of the electron. But in order to emulate the spherical distribution of charge experimentally measured and reported in the literature [13], an elliptical deformation parameter D must be introduced to the horn torus geometry to transform it into a horn spheroid as shown in fig. 6 and the corresponding parametric equations.

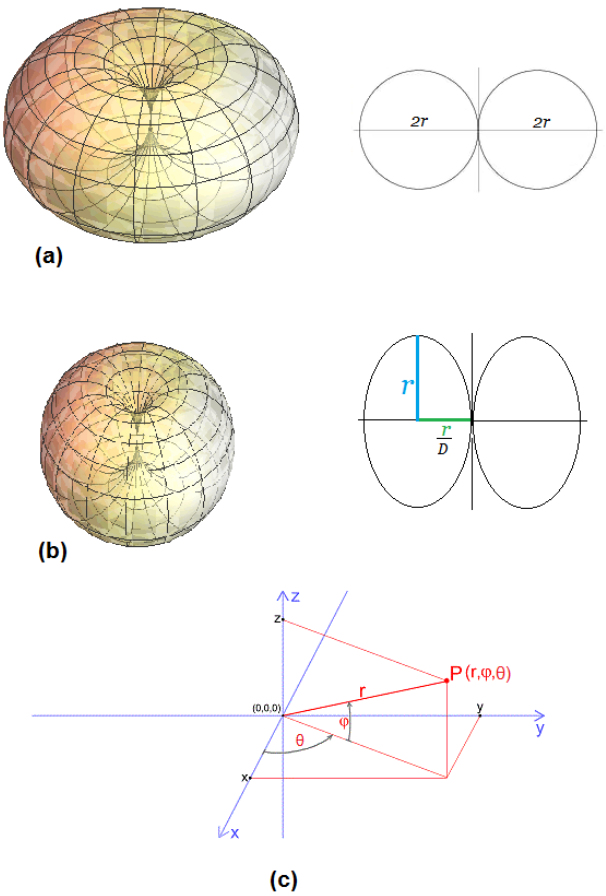

Fig. 6: Transformation of the horn torus topology into a horn spheroid to match the electron manifold. (a) General horn torus topology. (b) Horn Spheroid by applying a *D* elliptical deformation parameter. (c) The polar coordinates used in the parametric equations.

Horn spheroid parametric transformation equations,

$$x = \frac{r}{D}(1-\cos\varphi)\sin\theta \tag{16}$$

$$y = \frac{r}{D}(1-\cos\varphi)\cos\theta \tag{17}$$

$$z = r\sin\varphi \tag{18}$$

Where r, is the given radius and θ and φ the polar coordinates responsible for the F_S and F_R rotations in the manifold. Their angular velocities ratio is controlled by the $S=F_S/F_R$ parameter, previously introduced in equation (5).
The value of angle αº of the electromagnetic flux lines trajectory on the surface of the electromagneto sphere at the exact moment when crossing the equatorial plane at the center of the manifold, where the center of mass is also located inside the manifold, depends on both the values S and D chosen each time in the parametric equations. In fig.7 we can see geometrically for an infinitesimal small area on the surface of the manifold where the crossing happens and which can be considered therefore as a flat surface, the relation of the parameters S and D with the angle αº.

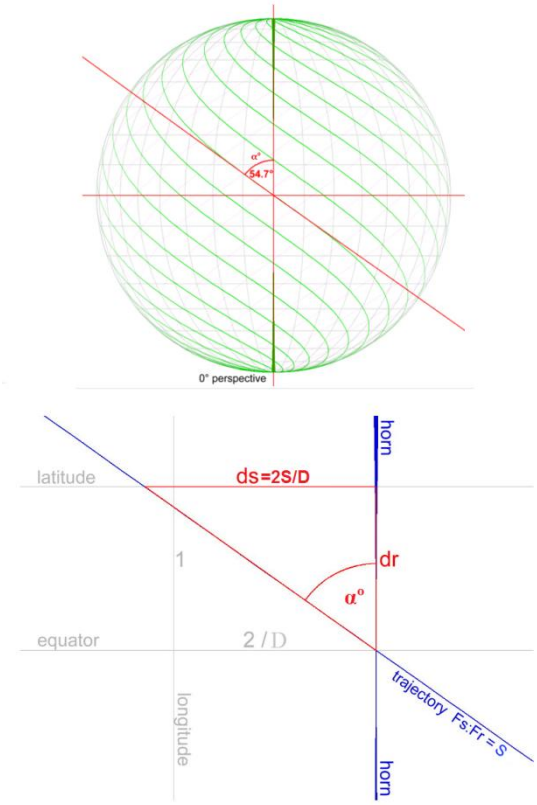

Fig. 7: Geometrical dependence of the electromagnetic flux line trajectory crossing the equator at the surface of the electromagneto sphere at an angle α°, with the $S=F_S/F_R$ and D parameters of the manifold's parametric equations. Notice, in the normal horn torus geometry without any deformation parameter D applied, the height to width radius ratio is 1:2.

As we observe in fig. 7, that tan α° = 2S/D, which means that we can work out for a given $S=F_S/F_R$ parameter, what the value of the deformation parameter D must be in order to achieve the exact magic angle α°=54.73561º value needed our manifold to have in order to pass the spin angular momentum consistency criterion check as analyzed by eq. (2)&(3) in section 2.2.
From our above analysis, the parametric equations (16), (17) and (18) for the proposed electron manifold can therefore be re-written in their complete form as following:

$$x = \frac{r}{D}(1-\cos\varphi)\sin(S\cdot\varphi) \tag{19}$$

$$y = \frac{r}{D}(1-\cos\varphi)\cos(S\cdot\varphi) \tag{20}$$

$$z = r\sin\varphi \tag{21}$$

$$\text{with } \theta = S\cdot\varphi \tag{22}$$

Also by adding the angle αº in our set of parameters for the electron manifold, we get:

$$\tan a = \frac{2S}{D}, \text{with } a^{\circ} = \arctan a \tag{23}$$

$$S = \frac{(\tan a)D}{2} \tag{24}$$

$$D = \frac{2S}{\tan a} \tag{25}$$

Next we will use equations (19) to (25) to calculate the exact manifold parameter values needed in order the manifold to be consistent with the spin angular momentum √2 criterion, see eq. (2)&(3), needed and also the light speed c consistency criterion, see eq. (4) we analysed previously in section 2.2.

3. Results and discussion

3.1. Wolfram simulations

In order the manifold to be consistent with theory it must pass both consistency checks criteria previously described at the beginning of section 2.2. Although finding the correct values for S and D parameters in order to achieve the magic angle [30] α°=54.73561° and therefore $L_R/L_S=\sqrt{2}$ (i.e. spin angular momentum consistency criterion check) is relatively an easy and straight forward task, applying equations (19) to (25), finding the correct combination of S and D parameters for the model to be in addition also fixed light speed c consistent thus, $F_S/F_R=P_R/P_S=Rr/Rs$ (i.e. fixed light speed c consistency check criterion) has proven more tricky, arbitrary and time consuming for deriving an analytic solution if there is one. Therefore we used Wolfram Alpha to simulate the results, thus the trajectory path (see fig. 3a) for each case of S and D values combination and finding the correct candidates for the proposed electron manifold herein. Almost two hundred simulation runs were performed manually and at the end we were able to narrow the band down to three cases of candidates. The simulation calculated the total path length of the trajectory of the F_R revolution through the horn tube of the manifold (see fig.3b) thus equivalent with $P_R=2\pi Rr$ perimeter, that allowed us to compare it with the known perimeter of the z-axis F_S spin rotation component of the magnetosphere around the magnetic moment N-S axis $P_S=2\pi Rs$, and therefore verify if the light speed c consistency criterion, $S=P_R/P_S$ checks out.

Most importantly, because the simulation simulates the actual helical type of trajectory of the F_R revolution for the manifold in contrast to the theoretical spin angular momenta calculations presented in section 2.2, which assume always for both F_S and F_R component rotations a circular loop path trajectory giving an effective value for F_S, F_R, R_S and Rr that would result on the known expected values of L_S and L_R, we are now able to feed in the actual simulated values result and recalculate using equations (7) and (13) (i.e. adapted each time for the different spins ½ and $1/\sqrt{2}$ of F_S and F_R), to see if our manifold candidate gives actually the correct values thus $L_R/L_S=0.707\hbar/0.5\hbar=\sqrt{2}$ and therefore complies also with the spin angular momentum consistency check. For the F_S spin rotation the theoretical effective values with the actual simulated are the same because F_S spin rotation has actually a circular loop trajectory in contrast to F_R rotation which is of a helical type.

a) Perfect Horn Sphere $S=\sqrt{2}$, α°=54.73561° (electron manifold candidate):

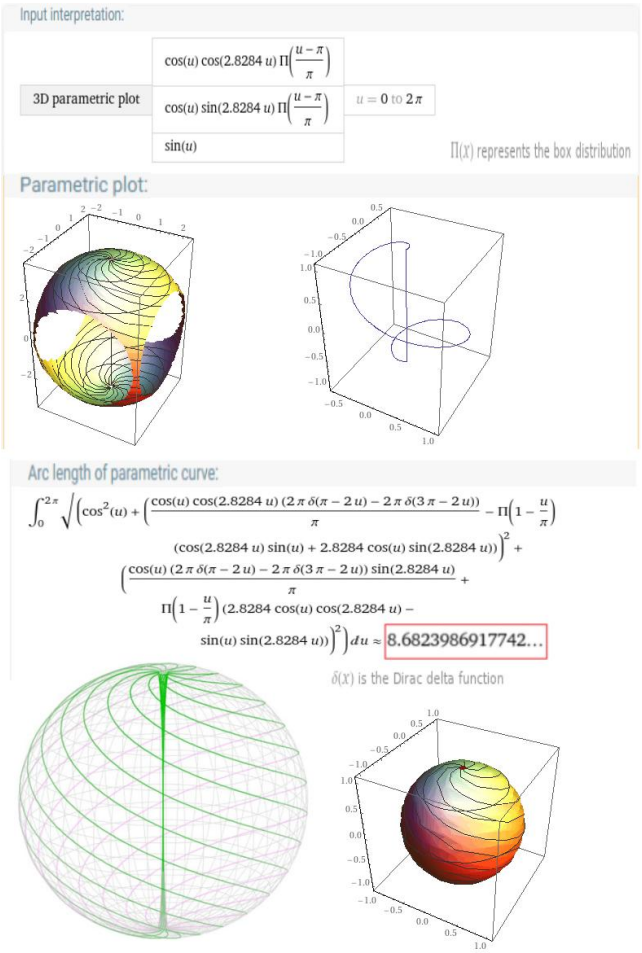

Fig. 8: Perfect horn sphere *S=√2* and radius *r=1*, Wolfram simulation

https://tinyurl.com/y8yfwtel (trajectory plot simulation)
https://tinyurl.com/y9odf6un (solid plot simulation)
https://tinyurl.com/y6vo89y9 (horn sphere animation)[7]

A perfect horn sphere can be regarded safely as a sphere with a very thin horn tube practically a straight line, joining its two poles, fig. 8. We had to modify the parametric equations for the horn spheroid (20), (21)&(22) to successfully simulate this candidate's manifold behavior in a continuous parametric equation so that Wolfram could also calculate the total path length value, shown in fig.8 outlined inside

[7] Permalink https://web.archive.org/web/20201231125958/https://www.horntorus.com/particle-model/greensphere.html

a red box, by adding the rectangular function rect(t)=Π(t) which by Fourier analysis transforms to a perfect line signifying an infinite frequency response at the region where the horn tube of the sphere is located through its two poles. This last point, makes much physical sense to the authors of this paper since the horn string of the electron manifold thus its magnetic moment, must respond to any external EM signal wave and therefore the electron must have ideally an infinite frequency bandwidth in this Universe. The angle α° in this topology since there is no deformation parameter D present, is given by tan α°= S with $S=F_S/F_R$. Please notice here, as shown in fig.8 of the parametric equations for the horn sphere compared to the horn spheroid equations (19) to (21) because the different geometry, in order to achieve the same $S=F_S/F_R$ ratio value and subsequent angle α° with the horn spheroid geometry, the chosen S parameter must be inputted in the horn sphere simulation multiplied by a factor of two. Thus, for S=√2=1.4142, the value 2.8284 must be inputted instead. In Wolfram polar coordinate angles φ° and θ° we used herein (see fig.6c) are named u and v (see fig. 8) accordingly.

The simulation run of the horn sphere shown in fig. 8 is for a given simulation radius r=1 (i.e. radius to the equator) in order to simplify at first the presentation here. Following, we will present the results for radius the theoretical calculated in section 2.2, Fs spin rotation radius, numerically $r=R_S$ =3.344. For simplification most of the results are presented only numerically without units attached or exponentials and only the sim input data and output end data are presented herein. The complete set if simulation data can be found in the supplementary material of this research referenced here [28].

Simulation input: S= √2=1.4142 (α°= 54.73561°), r=rs=3.344.

Output:

P_R= 2π Rr =29.033 → Rr= 4.62 ((predicted value for helical path 4.72, predicted for circular path 6.46)

Simulated L_R value for F_R =Fs/√2 =142.67E18/ √2 =100.88E18 Hz

L_R = (0.707 x h x Fs/c) x Rr = (0.707 x 6.626 x 100.88 / 2.99) x 4.62 = 0.730 (predicted 0.707xħ =0.707x1.054= 0.745)

Simulated result: Manifold passed both consistency criteria.

Notice here from the above results how the helical path of the F_R revolution is able to produce approximate the predicted by theory L_R value with less actual radius Rr(act)=4.62 than the theoretical predicted 6.46. This is because the actual F_R value was increased to F_R(act)=100.88 from the predicted theoretical 73.85 calculated in section 2.2, eq. (15). This phenomenon is known that a helix motion for the same cylindrical radius and tangential velocity with a circular loop both having the same effective perimeter thus total trajectory path length, produces more angular velocity acting like an angular velocity amplifier and therefore can generate more spin angular momentum (i.e. not to be confused with the situation described in section 2.2 of the comparison of the total spin angular momentum of the electron ≈0.866h with the spin angular momentum of a photon, ħ).

b) Horn Spheroid S=√2, D=2, α°=54.73561° (electron manifold candidate):

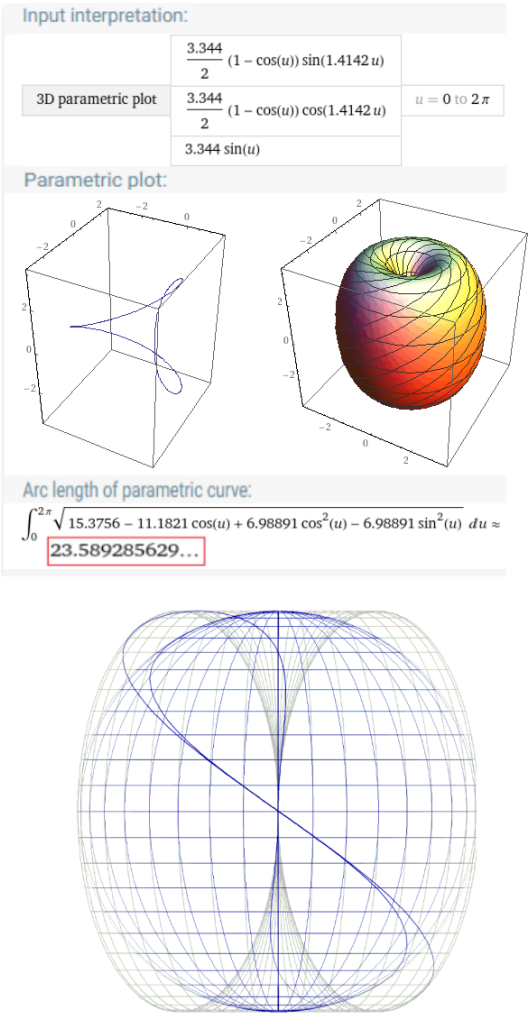

Fig. 9: Horn Spheroid S=√2, D=2 and radius r=3.344 Wolfram simulation

https://tinyurl.com/yd8uyo93 (trajectory plot simulation)
https://tinyurl.com/ycepyayp (solid plot simulation)

We see also here, that in this case although the magic angle was implemented α°=54.7361° the manifold failed even to generate the known value of L_R=0.707ħ. This is because the volume of the horn spheroid exceeded the volume of a sphere with the same radius to the equator, see fig. 9.

This horn spheroid topology of elliptical deformation D=2, is the closest a horn torus can get to an actual sphere. We see in fig. 9 the previous perfect horn sphere overlaid with the D=2 horn spheroid both having the same radius to the equator and the same parameter S=√2=1.4142. Also in the same illustration we can observe the trajectories plotted of these two different manifold candidates. The following simulation end results were produced for radius r=3.344 to the equator.

S=Fs/Fr=1.41 ≠ Pr/Ps =23.589/21.0109=1.122 since the Ps=21.0109 with r=3.344

Actual P_R=2piRr = 23.589 → r_R= 3.754 → L_R=0.593 (theoretical predicted 0.745) (failed known prediction)

Simulated Result:

P_R/Ps=1.12 ≠ Fs/Fr=S=√2=1.4142 (failed light speed c consistency criterion check).

Also generated L_R/Ls=1.12 ≠ √2 (failed the spin angular momentum consistency criterion check).

c) Golden Mean Horn Spheroid D=Φ=1.618, S=1.1441 ≈7/6, α°=54.73561° (electron manifold candidate):

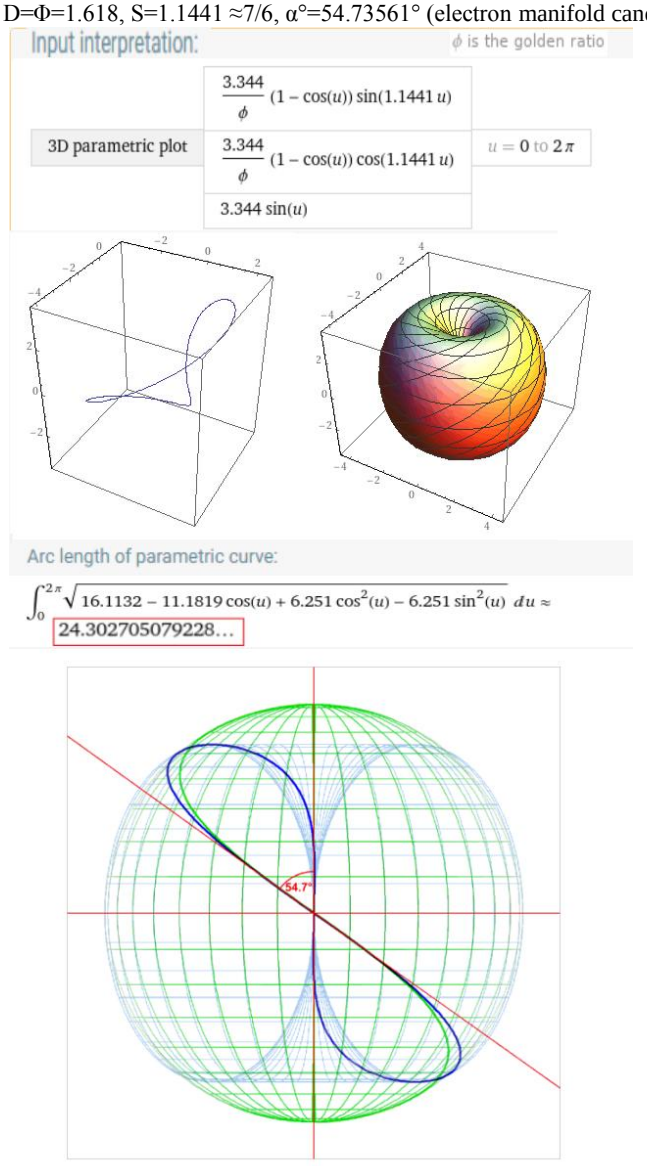

Fig. 10: Golden Mean Horn Spheroid S=1.1441≈7/6, D=Φ=1.618 and radius r=3.344 Wolfram simulation

https://tinyurl.com/ybmn2q4x (trajectory plot simulation)
https://tinyurl.com/y7zw43k4 (solid plot simulation)
https://tinyurl.com/y8zpnsa8 (horn spheroid animation)[8]

The authors of this paper although do not pay any particular attention to the various 'theories' about the importance of the golden mean Φ and how it can be found 'everywhere in nature', were surprised that this specific candidate, after almost 200 simulation runs experimenting with different parameter values each time, was the only horn spheroid geometry fig. 10, which passed all the criteria consistency checks and also generated the correct, known, spin angular momenta values. The Wolfram simulation end results are shown as following.

Simulation input: S= 1.1441 (α°= 54.73561° Le^Ls), r=rs=3.344, D=Φ(golden ratio)=1.61803398875

Output:

P_R= 2π Rr =24.3027 → Rr= 3.8678 Compton Radius for the electron! (Predicted value for circular path 6.46)

Simulated L_R value for F_R =Fs/1.1441 =142.67E18/ 1.1441 =124.7E18 Hz

L_R = (0.707 x h x Fs/c) x Rr = (0.707 x 6.626 x 124.7 / 2.99) x 3.8678 = 0.755 (predicted 0.707xħ =0.707x1.054= 0.745)

[8] Permalink https://web.archive.org/web/20201231132316/https://www.horntorus.com/particle-model/phi-hornspheroid_6-7.html

Simulated result: Manifold passed both consistency criteria.
This manifold is validated as a strong candidate for the electron. It also passes the light speed c consistency check since $S=Fs/F_R = P_R/Ps = 1.15$.
As in the case of the √2 perfect horn sphere, it also generates $L_R/Ls=\sqrt{2}$.

3.2. Choosing the best manifold candidate for the electron

Summarizing the results of the previous section 3.1 we get Table.1:

Table 1: Final Electron Manifold Candidates

Candidate	Spin Angular Momentum Check	Light Speed c Consistency Check
Horn Sphere S=√2	Pass	Pass
Horn Spheroid S=√2, D=2	Fail	Fail
Horn Spheroid S=1.1441, D=Φ	Pass	Pass

We are left with two manifold candidates for the electron to choose shown in Table.1. The perfect horn sphere and the golden mean Φ horn spheroid. The perfect horn sphere is more like an absolute ideal mathematical model whereas the golden mean horn spheroid is a more natural thus physical. However, there could be two more clues hidden in our analysis and simulation results that might be in favor for the golden horn spheroid manifold as the best candidate for the electron. The simulation results showed for the golden spheroid an actual effective circular path radius for the F_R revolution of Rr=3.86E-13 m, which coincides with the Compton radius Rc reported in literature as we previously referenced and derived from the Compton wavelength λc for the electron, thus its photon energy equivalent. In our theoretical paper herein and electron manifold described we have shown previously in this animation of virtual photons exchange between electrons, see animation here https://tinyurl.com/y8hqa6sp, of how the ½ spin manifold energy ribbon inside the electron, which is actually a ½ spin spatially twisted photon in 3D space, unfolds when ejected to a spin 1 circular 2D loop manifold photon of Rc=Rre=3.86E-13 m Compton radius photon. The effective circular loop radius Rr_e of the F_R revolution of our electron manifold that we found in our simulation results to be equal to the well reported Compton radius and Compton wavelength $\lambda c=2\pi Rc=2\pi Rre$, is an indication that the golden mean horn spheroid might be the best suitable manifold for describing the electron.
Besides that, we found in the simulation results of the golden spheroid an actual angular velocity frequency F_R for the golden mean spheroid to be 124.7E18 Hz, the same as the known value of the γ-ray emission frequency from the annihilation of an electron-positron pair. As a downside, we must say here that the geometry of the golden spheroid is not complete spherical that would contradict with the reported and measured with high accuracy spherical distribution of electron charge as we referenced previously [13]. Nevertheless, this relativistically spinning spheroid could create a smearing effect on the poles that would anticipate any non uniformity in geometry. Also the angular velocity approaching the two pole apertures of the relativistic manifold golden horn spheroid, increases substantially more than in the case of the perfect horn sphere. That could also counterbalance the loss of geometric uniformity thus charge distribution in 3D space. Last but not least, the combined FS≈142 EHz (exahertz) and FR≈124 EHz simulated values in our proposed manifold can account for the reported in literature Zitterbewegung value of the electron predicted at $2mec^2/\hbar\approx254$ EHz considering also that the manifold is not completely spherical.

3.3. Fine structure constant of the electron manifold

The authors' hypothesis in this research presented herein and supported by an analysis which can be found in the supplementary material [28] of this research as an Appendix, is that the Fine Structure Constant [33] (FSC) α, is embedded as a proportionality constant in the topology of the electron spin relativistic electromagnetic flux manifold.
Geometrically it could be described, as the ratio of the diameter of the horn tube at the pole (i.e. thickness of vortex string, magnetic moment, joining the two poles N-S) to the diameter of the electron's magnetosphere (i.e. charge) at the equator:

$$\alpha = \left(\frac{\text{diameter of horn tube of electron}}{\text{diameter at equator of electron}} \right) \approx \frac{1}{137} \tag{26}$$

Approximately, the diameter of the horn tube is therefore 0.7% the diameter of the electron at its equator. This topology proportionality constant is always kept even when the electron is not at rest and strongly interacting with the environment and other particles except of course the case of an electron-positron pair annihilation.
We can demonstrate this concept of the FSC α as a topological proportionality feature in fig. 11.

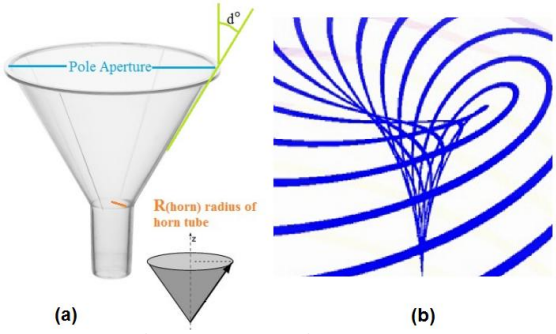

Fig. 11: Horn funnel with horn tube shown in the topology of the electron manifold at its N and S pole regions. (a) Illustration of a cone funnel geometry with a tube connected at its end as an approximation of the electron's manifold polar region horn funnel continuing as a horn tube or else called vortex string at the end. The pole aperture diameter D of the funnel and the horn tube radius R(horn) are demonstrated as well as the cone angle d° as an average angle of the actual elliptical cone structure of the polar horn funnel in the manifold. (b) Actual horn funnel in the electron manifold ending up to a very thin horn tube or else called vortex string. A complete approximate analysis of this topology and its proposed relation with the fine structure constant can be found at the supplementary material of this research [28]).

We were also able to derive from the geometrical features and analysis of the horn funnel and horn tube topology demonstrated in fig. 11, an approximation equation shown below that calculates the horn tube radius R(horn) in the proposed electron manifold , given the values for the pole aperture D and angle d° (see fig. 11):

$$R(\text{horn}) = \frac{D}{2} \cdot \left(\frac{\tan(d)}{\sin(d)} - 1 \right) \tag{27}$$

From equation (27) shown above and successfully extrapolating from the manifold using the Wolfram simulation, the pole aperture value D and assuming our fine structure constant hypothesis as a topological proportionality constant of our manifold is correct thus R(horn) must be using eq. (26), R(horn) ≈ (electron radius at equator) / 137, we succeeded in calculating the average angle d° of the horn funnel structure in our proposed manifold the golden mean horn spheroid by solving the trigonometric equation (27) for angle d°. This solution resulted to an angle value:

$$d° = 28.13900271 \tag{28}$$

The complete analysis of this calculation can be found in the supplementary material [28] of this research as an Appendix.

3.4. Lorentz group interpretation of the electron's topology

In mathematics and mathematical physics the Standard Model (SM) of quantum mechanics and consequently the electron is described as part of the Lorentz group that obeys the quadratic equation on R^4:

$$(t, x, y, z) \mapsto t^2 - x^2 - y^2 - z^2 \tag{29}$$

The four connected components are not simply connected [34] and therefore this strongly infers that in the three-dimensional Euclidean space the electron would have a non simply connected 3D topology, see fig.12.

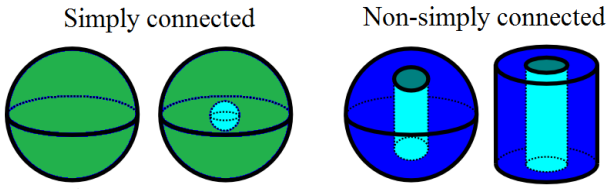

Fig. 12: Examples of Simply Connected vs. Non-Simply Connected 3D Euclidean Topologies.

The hollow sphere shown in the illustration of fig. 12, would then represent the charge of the electron and the pipe running throughout the diameter of the sphere from pole to pole represents the magnetic dipole moment of the electron. This Lorentz group geometric algebra description translated into differential geometry is in agreement with our proposed topology and manifold for the electron. In addition, it explains the intrinsic quantum spin of the electron and also maybe for the first time gives a classical explanation, of why the electron's quantum spin magnetic moment is almost twice, g-factor≈2 the expected classical value, since it clearly suggests that by classical interpretation, the nature of the magnetic dipole moment of the electron may not be Amperian as initially thought but instead Gilbertian as we have analyzed previously in section 2.1.

4. Conclusions

We have herein proposed a complete description and analysis and quantum theory for inside the electron, beyond quantum mechanics standard model (SM), of a possible topology and manifold of the free electron at rest as an isolated closed system based on actual indirect and non-intrusive physical observations and our previously published experimental research [21]. Our view inside the electron and its intrinsic manifold is macroscopic, the only kind of view we are made to really physically comprehend and decipher its otherwise only mathematically abstract described quantum intrinsic properties and forced to accept by the SM without a physical explanation like for example the proposition "it has a spin but without physically spinning". The authors of this paper and research suggest that there is no really any other way to continue today to progress general physics theories of the quantum world and make theoretical and technological breakthroughs and go to the next step, without first decipher and physically explain the origin of these intrinsic properties of elementary particles like the electron, thus the origin of its spin, charge, magnetic moment, handedness, helicity and even its mass inertia which is described today by the Higgs Mechanism and Higgs field and experimentally confirmed but leaves questions unanswered for example for the electron, how such a dimensionless mass can have such a relative low energy, 511KeV? Which is a contradiction in the general quantum theory, SM and high-energy physics. This kind of questions the authors of this paper suggest can only be answered by assigning an energy flow manifold and topology to elementary particles (including the Higgs Boson) starting with the electron and connecting their measured intrinsic properties with their manifold features so that they can physically deciphered and explained. Maybe this is the missing link and information missing we need to explain most of the unanswered questions and "mysteries" of physics today. It may that, the answer of why we did not find SUSY yet (for the last eight years now), is hidden inside the electron. It is a hard task but we must try anyway. Moreover, fundamental constants of the quantum but also extended and tremendously impacting the macrocosm like the fine structure constant, its origin can be hidden inside the energy flow manifold of the electron.

We have shown here in this research, how and why all the intrinsic properties of the electron can be interpreted as topological and geometrical features of its proposed manifold and fiber model. Importantly, we have demonstrated how all of the intrinsic properties of the electron are generated and can be calculated and simulated in our fiber model by the clockwork spin relativistic speed, rotational and revolution vibrational motion of a single fiber spinor (see energy ribbon of fig.3a and its linked dynamic animation) without any translational motion involved and therefore we have shown the common origin of these properties and the underlying interconnected mechanics that correlate them together. Furthermore, we have demonstrated, because this single energy ribbon of fig.3a vibrates both longitudinally

and latitudinally at the same time at relativistic speed, how it creates the magnetosphere and charge of the electron particle at rest, see fig.3b&c and linked animation. By studying our electron manifold, we give an explanation why the electron appears to have a dimensionless mass but in the same time has a charge radius and occupies a volume in three-dimensional Euclidean space. At the end, we show how the fine structure constant may be embedded inside the electron as a topological feature and proportionality constant of the electron manifold ultimately deciphering its origin and additionally why our proposed electron topology complies with the Lorentz group. The basis of our spin relativistic manifold of the electron is a vibrating ½ spin closed loop quantum string (i.e. fiber) of electromagnetic flux (i.e. the concept of electromagnetic flux lines as relativistic strings in not new [35]). Thus, actually a spin ½, twisted spatially in three-dimensional Euclidean space (see fig.3a) photon.

An important conclusion overall from our research (see sections 1&2.1) was made that elementary particles in order to interact with the Higgs field and gain their mass inertia must occupy a volume in tree-dimensional Euclidean space. This conclusion is reinforced by relative recent experimental findings published by independent sources [36 - 38] that electrons in atomic thin layers of graphene behave like massless particles thus when electrons are forced into a practically 2D surface medium environment without volume, they behave more like photons. This strongly suggests that electrons cannot be regarded as dimensionless mass particles as initially thought but have an associated energy topology and manifold occupying a volume in space. Similarly, we deduce that photons must essentially have a two-dimensional topology in space and therefore do not have a volume (see fig.3d). Our research presented herein is elementary a complete physical novel description of the electron as a four-dimensional quantum string spinor.

In our presented research we examine a possible Quantum Topology and dynamic manifold for the free electron at rest. Meaning we assume and examine the ideal case of an isolated electron with spin relativistic motion but no translational linear motion. Under these conditions, QM does not make any predictions about the probabilistic nature of the electron, there is no conflict with the theory and deterministic intrinsic mechanics in the case of the single isolated electron are possible. The possible deterministic nature of single isolated closed system elementary particles are also strongly inferred from our consistent experience of measuring very accurately the fixed values of their intrinsic properties like spin, charge, mass, magnetic moment etc. If ontologically, single elementary particles would be probabilistic in nature then why are we measuring these same exact values every time we measure them? This surely implies deterministic mechanics and the SM model does not give answer of what an isolated elementary particle intrinsic mechanics would be?

Our presented research is not just novel but also we believe opens up a new field of Quantum Topology into elementary particles intrinsic mechanics, high energy theoretical research and phenomenology. We have made the beginning with the lightest of the charged particles, the electron.

In the supplementary material [28] of this research you will find all the Appendix of this paper with calculations and further analysis supporting our findings and conclusions herein as well as preliminary outlined descriptions of the implications of our novel intrinsic fiber model of the electron has on solving and explaining quantum phenomena which are regarded until today of not having a classical solution and explanation. Therefore, further supporting and demonstrating the validity and merits of our research.

Acknowledgements

Many thanks to Professor Cristian Lăzureanu of the Polytechnic University of Timisoara Department of Mathematics, for our fruitful discussion and his support. Exceptional thanks to Mr. Wolfgang W. Däumler, mathematical animations expert and university trained physicist, creator of the artmetic animation software engine and horntorus.com site, who has created generously all the animations of our proposed manifold, few of them are referenced here in this paper and overall for his support and great interest he showed for our research.

Declarations

The authors have no relevant financial or non-financial interests to disclose.
The authors did not receive support from any organization for the submitted work.
The datasets generated during and/or analysed during the current study are available in the google drive repository [28], https://drive.google.com/drive/folders/1jLVe5AKSOlsU7VH-r_QJ2tuLwtbFkjpS

References

[1] G.E. Uhlenbeck, S. Goudsmit, Ersetzung der Hypothese vom unmechanischen Zwang durch eine Forderung bezüglich des inneren Verhaltens jedes einzelnen Elektrons, Naturwissenschaften. 13 (1925) 953–954. https://doi.org/10.1007/BF01558878.
[2] G.E. UHLENBECK, S. GOUDSMIT, Spinning Electrons and the Structure of Spectra, Nature. 117 (1926) 264–265. https://doi.org/10.1038/117264a0.
[3] L.H. THOMAS, the Motion of the Spinning Electron, Nature. 117 (1926) 514. https://doi.org/10.1038/117514a0.
[4] P. ZEEMAN, the Effect of Magnetisation on the Nature of Light Emitted by a Substance, Nature. 55 (1897) 347. https://doi.org/10.1038/055347a0.
[5] P. Zeeman, VII. Doublets and triplets in the spectrum produced by external magnetic forces , London, Edinburgh, Dublin Philos. Mag. J. Sci. 44 (1897) 55–60. https://doi.org/10.1080/14786449708621028.
[6] T. Preston, Radiation Phenomena in a Strong Magnetic Field, in: Sci. Trans. R. Dublin Soc., Royal Dublin Society, Dublin, 1898: pp. 385–389.
[7] W. Gerlach, O. Stern, Der experimentelle Nachweis der Richtungsquantelung im Magnetfeld, Zeitschrift Für Phys. 9 (1922) 349–352. https://doi.org/10.1007/BF01326983.
[8] W. Gerlach, O. Stern, Das magnetische Moment des Silberatoms, Zeitschrift Für Phys. 9 (1922) 353–355. https://doi.org/10.1007/BF01326984.
[9] D.J. Griffiths, Introduction to Quantum Mechanics, in: Prentice Hall, New Jersey, 1995: p. 155.
[10] A.H. Compton, The size and shape of the electron, Phys. Rev. 14 (1919) 20–43. https://doi.org/10.1103/PhysRev.14.20.
[11] M.H. Mac Gregor, the Enigmatic Electron, in: Klurer Academic, Boston, 1992: pp. 4–5. https://doi.org/10.1007/978-94-015-8072-4.
[12] M.H. MacGregor, the Enigmatic Electron: A Doorway to Particle Masses, 2nd ed., El Mac Books, Santa Cruz, CA, 2013.
[13] V. Andreev, D.G. Ang, D. DeMille, J.M. Doyle, G. Gabrielse, J. Haefner, N.R. Hutzler, Z. Lasner, C. Meisenhelder, B.R. O'Leary, C.D. Panda, A.D. West, E.P. West, X. Wu, A. Collaboration, Improved limit on the electric dipole moment of the electron, Nature. 562 (2018) 355–360. https://doi.org/10.1038/s41586-018-0599-8.
[14] P. Schattschneider, C. Hébert, H. Franco, B. Jouffrey, Anisotropic relativistic cross sections for inelastic electron scattering, and the magic angle, Phys. Rev. B - Condens. Matter Mater. Phys. 72 (2005) 045142. https://doi.org/10.1103/PhysRevB.72.045142.
[15] H. Daniels, A. Brown, A. Scott, T. Nichells, B. Rand, R. Brydson, Experimental and theoretical evidence for the magic angle in transmission electron energy loss spectroscopy, in: Ultramicroscopy, Elsevier, 2003: pp. 523–534. https://doi.org/10.1016/S0304-3991(03)00113-X.

[16] B. Jouffrey, P. Schattschneider, C. Hébert, The magic angle: A solved mystery, Ultramicroscopy. 102 (2004) 61–66. https://doi.org/10.1016/j.ultramic.2004.08.006.
[17] M. Bydder, A. Rahal, G.D. Fullerton, G.M. Bydder, The magic angle effect: A source of artifact, determinant of image contrast, and technique for imaging, J. Magn. Reson. Imaging. 25 (2007) 290–300. https://doi.org/10.1002/jmri.20850.
[18] W. Heisenberg, Über den anschaulichen Inhalt der quantentheoretischen Kinematik und Mechanik, Zeitschrift Für Phys. 43 (1927) 172–198. https://doi.org/10.1007/BF01397280.
[19] M. Schlosshauer, Decoherence, the measurement problem, and interpretations of quantum mechanics, Rev. Mod. Phys. 76 (2005) 1267–1305. https://doi.org/10.1103/RevModPhys.76.1267.
[20] M. Schlosshauer, Decoherence and the Quantum-To-Classical Transition, Springer, Berlin Heidelberg, 2008. https://doi.org/10.1007/978-3-540-35775-9.
[21] E. Markoulakis, A. Konstantaras, J. Chatzakis, R. Iyer, E. Antonidakis, Real time observation of a stationary magneton, Results Phys. 15 (2019) 102793. https://doi.org/10.1016/j.rinp.2019.102793.
[22] G. Aad, T. Abajyan, B. Abbott, et al., Observation of a new particle in the search for the Standard Model Higgs boson with the ATLAS detector at the LHC, Phys. Lett. Sect. B Nucl. Elem. Part. High-Energy Phys. 716 (2012) 1–29. https://doi.org/10.1016/j.physletb.2012.08.020.
[23] P.W. Higgs, Broken symmetries and the masses of gauge bosons, Phys. Rev. Lett. 13 (1964) 508–509. https://doi.org/10.1103/PhysRevLett.13.508.
[24] E. Markoulakis, J. Chatzakis, A. Konstantaras, E. Antonidakis, A synthetic macroscopic magnetic unipole, Phys. Scr. 95 (2020) 095811. https://doi.org/10.1088/1402-4896/abaf8f.
[25] E. Markoulakis, A. Konstantaras, E. Antonidakis, The quantum field of a magnet shown by a nanomagnetic ferrolens, J. Magn. Magn. Mater. 466 (2018) 252–259. https://doi.org/10.1016/j.jmmm.2018.07.012.
[26] E. Markoulakis, I. Rigakis, J. Chatzakis, A. Konstantaras, E. Antonidakis, Real time visualization of dynamic magnetic fields with a nanomagnetic ferrolens, J. Magn. Magn. Mater. 451 (2018) 741–748. https://doi.org/10.1016/j.jmmm.2017.12.023.
[27] D. Vasyukov, Y. Anahory, L. Embon, D. Halbertal, J. Cuppens, L. Neeman, A. Finkler, Y. Segev, Y. Myasoedov, M.L. Rappaport, M.E. Huber, E. Zeldov, A scanning superconducting quantum interference device with single electron spin sensitivity, Nat. Nanotechnol. 8 (2013) 639–644. https://doi.org/10.1038/nnano.2013.169.
[28] E. Markoulakis, - Google Drive Supplementary Material, https://tinyurl.com/y8guqn5c(short link), https://drive.google.com/drive/folders/1jLVe5AKSOlsU7VH-r_QJ2tuLwtbFkjpS (long link), (accessed April 27, 2021).
[29] W. Gilbert, De magnete, Dover Publications, New York, 1958. https://tinyurl.com/y9ljreyt (accessed December 17, 2020).
[30] Y. Cao, V. Fatemi, S. Fang, K. Watanabe, T. Taniguchi, E. Kaxiras, P. Jarillo-Herrero, Unconventional superconductivity in magic-angle graphene superlattices, Nature. 556 (2018) 43–50. https://doi.org/10.1038/nature26160.
[31] A. Gray, E. Abbena, S. Salamon, Modern Differential Geometry of Curves and Surfaces with Mathematica, in: 3rd ed., CRC Press, Boca Raton, FL, 2006: pp. 305–306.
[32] C. Lăzureanu, Spirals on surfaces of revolution, VisMath, Math. Inst. SASA, Belgrade. (2014). http://elib.mi.sanu.ac.rs/pages/browse_issue.php?db=vm&rbr=57 (accessed December 20, 2020).
[33] A. Sommerfeld, Zur Quantentheorie der Spektrallinien, Ann. Phys. 356 (1916) 125–167. https://doi.org/10.1002/andp.19163561802.
[34] S. Weinberg, the Quantum theory of fields. Vol. 1: Foundations, Cambridge University Press, 2005.
[35] L.J. Tassie, Magnetic flux lines as relativistic strings, Phys. Lett. B. 46 (1973) 397–398. https://doi.org/10.1016/0370-2693(73)90150-0.
[36] M. Wilson, Electrons in atomically thin carbon sheets behave like massless particles, Phys. Today. 59 (2006) 21–23. https://doi.org/10.1063/1.2180163.
[37] S. Chen, Z. Han, M.M. Elahi, K.M.M. Habib, L. Wang, B. Wen, Y. Gao, T. Taniguchi, K. Watanabe, J. Hone, A.W. Ghosh, C.R. Dean, Electron optics with p-n junctions in ballistic graphene, Science (80-.). 353 (2016) 1522–1525. https://doi.org/10.1126/science.aaf5481.
[38] H. Yoon, C. Forsythe, L. Wang, N. Tombros, K. Watanabe, T. Taniguchi, J. Hone, P. Kim, D. Ham, Measurement of collective dynamical mass of Dirac fermions in graphene, Nat. Nanotechnol. 9 (2014) 594–599. https://doi.org/10.1038/nnano.2014.112.